Numerical study on convective heat transfer of supercritical CO$_2$ in vertically upward and downward tubes

YAN ChenShuai[1], XU JinLiang[1,2*], ZHU BingGuo[1], HE XiaoTian[1] & LIU GuangLin[1]

[1] *Beijing Key Laboratory of Multiphase Flow and Heat Transfer for Low Grade Energy Utilization, North China Electric Power University, Beijing 102206, China;*
[2] *Key Laboratory of Power Station Energy Transfer Conversion and System, Ministry of Education, North China Electric Power University, Beijing 102206, China*

The experimental measurement of supercritical pressure carbon dioxide (sCO$_2$) heat transfer in vertical downward flow was performed in a circular tube with inner diameter of 10 mm. Then, a three-dimensional numerical investigation of sCO$_2$ heat transfer in upward and downward flows was performed in a vertical heated circular tube. The influence of heat flux, mass flux, and operating pressure on heat transfer under different flow directions were discussed. According to the "pseudo-phase transition" viewpoint to supercritical fluids, the analogy to the subcritical inverted-annular film boiling model, the physical model to sCO$_2$ heat transfer was established, where fluid region at the cross-section of circular tube was divided into gas-like region covering heated wall and core liquid-like phase region. Then, the thermal resistance mechanism which comprehensively reflected the effect of multiple factors including the thickness of the gas-like film or liquid-like region, fluid properties and turbulence on heat diffusion was proposed. Surprisingly, thermal resistance variation in upward flow is well identical with that of wall temperature and heat transfer deterioration is predicted successfully. In addition, compared with thermal resistance in the core liquid-like region, gas-like film formation is determined to be the primary factor affecting heat transfer behavior. Results also show that total thermal resistance in upward flow is always larger than that in downward flow. The investigation can provide valuable guide to design and optimize sCO$_2$ heaters.

supercritical CO$_2$, flow direction, pseudo-film heat transfer, thermal resistance

1 Introduction

Supercritical CO$_2$ (sCO$_2$) Brayton cycle has drawn more and more attention for power conversion systems, such as next-generation nuclear reactor, coal-fired power plant, solar energy, and geothermal energy systems [1–4]. In this cycle system, the endothermic process of CO$_2$ in a specified heat exchanger can be regarded as being at constant pressure. The physical properties of supercritical fluids will dramatically change in a narrow temperature range, especially in the

neighborhood of pseudo-critical points. The phenomenon results in the complexity of supercritical heat transfer [5,6]. Consequently, as one of the key issues for the new power generation technology, it is crucial to thoroughly understand the heat transfer characteristic of sCO$_2$ for designing the heat exchangers in the sCO$_2$ Brayton cycle system [7]. As the promising candidates for recuperators in sCO$_2$ Brayton cycles, heat transfer characteristics of printed circuit heat exchangers employing various channels, such as airfoil shape fin, sinusoidal and zigzag channels has been extensively investigated [8,9].

For supercritical heat transfer in a vertical straight tube,

Pioro and Duffey [10] reviewed extensive experimental investigations and concluded that there exist three heat transfer modes, namely heat transfer enhancement (HTE), normal heat transfer (NHT), and heat transfer deterioration (HTD). As mentioned in the textbook, the gas-liquid coexistence state will terminate at the critical point, and from the perspective of physical phenomena, the liquid phase and gas phase cannot be distinguished under supercritical state. As a result, the supercritical fluid is regarded as single-phase fluid. Based on the above viewpoint, numerous scholars investigated heat transfer characteristic of supercritical fluids in the vertical tube. The flow acceleration and buoyancy effects were considered to be the main reasons to result in the HTD phenomenon. Simultaneously, some researchers [11–13] explained the buoyancy effect being the main mechanism leading to HTD by analyzing the effect of flow direction on supercritical heat transfer in a vertical tube. However, Shiralkar and Griffith [14,15] performed experiments with sCO_2 flowing vertically upward and downward in a circular tube. They found that HTD emerged in both upward and downward flows, and concluded that HTD was caused by a fluid layer with low density and low thermal conductivity in the near wall region. Wang et al. [16] experimentally and numerically analyzed the heat transfer characteristic of supercritical water, they considered that there existed other mechanisms resulting in HTD besides the buoyancy effect. However, they did not further reveal and analyze the mechanisms. Fan and Tang [17] numerically investigated the heat transfer characteristics of sCO_2 in a heated vertical tube. They considered that the local thicker thermal and flow boundary layers seem to cause the occurrence of HTD. Kim et al. [18] evaluated turbulent heat transfer to sCO_2 flowing under different directions in a circular tube and found that a remarkable wall temperature peak appeared in upward flow but disappeared in downward flow. Kim et al. proposed that flow acceleration was a prominent factor in this phenomenon. In general, it can be found that the viewpoints on the causes of abnormal heat transfer are inconsistent. In addition, the recent research results from Shen et al. [19] and Zhang et al. [20] showed that both buoyancy and flow acceleration effects cannot perfectly illustrate HTD phenomenon of supercritical fluids. And Xie et al. [21] also considered that it is equivocal whether the buoyancy and flow acceleration effects induced HTD. The above review provides the incentive to further explore the mechanism of sCO_2 heat transfer for engineering design.

Holman et al. [22] experimentally studied the flow and heat transfer of Freon 12 and visually detected that vapor trails appeared near the vertical wall. Although the vapor-liquid interface cannot be distinguished obviously under supercritical state, Holman et al. suggested that it should be justifiable to define this phenomenon as "pseudo-boiling". Likewise, Ackerman [23] qualitatively believed that char-acteristic of supercritical fluids heat transfer was similar to subcritical film boiling, which was considered as the main HTD mechanism. Unfortunately, Ackerman did not further analyze the mechanism in detail. Besides, in our previous research [24], from the perspective of liquid-like transiting to gas-like at pseudo-critical point, heat transfer behavior of sCO_2 flowing upward in a vertical tube is numerically investigated, and it is proposed qualitatively that the occurrence of HTD seemed to be mainly related to the gas-like film covering tube wall as well as the turbulence intensity in the core liquid-like region.

The present investigation is chiefly focused on numerically analyzing turbulent heat transfer to sCO_2 in the vertical tube under different flow directions to examine and identify influence factors of sCO_2 heat transfer. At present, the experimental data of sCO_2 in downward flow are rare and is mainly measured from micro-tubes with inner diameter 0.27–4.5 mm [18,25–27]. And thus, the main content is briefly organized as below in the present research. Initially, experimental measurement of sCO_2 heat transfer in vertical downward flow is performed in circular tube with inner diameter of 10 mm. Secondly, according to the viewpoint that sCO_2 will undergo "pseudo-phase transition" near pseudo-critical temperature, the characteristic of physical properties to sCO_2 and the static heat transfer model is laconically described. Thirdly, the influence of flow direction on sCO_2 heat transfer under different heat fluxes, mass fluxes, and pressures are discussed. Finally, based on the viewpoint of pseudo-film heat transfer, the thermal resistance theory which comprehensively reflects the effect of multiple factors including the thickness of gas-like film or liquid-like region, fluid properties, and turbulence on heat diffusion is proposed for supercritical heat transfer in this paper. HTD mechanism and the reasons for disparity of heat transfer between upward and downward flows are successfully explained. It is indirectly proved that the supercritical pseudo-film heat transfer model is reasonable.

2   Idealized physical model of heat transfer

Owing to different understanding of the physical properties of supercritical fluids, similar to the phenomenon of vapor-liquid transition at subcritical pressures, some researchers [28–30] proposed that supercritical fluids exhibit the characteristic of liquid-like and gas-like on both sides of the Widom line (WL), respectively. Figure 1(a) shows that an identifiable transition exists between the liquid-like phase and the gas-like phase near the WL. Note that WL is composed of maximum specific heat c_p at different supercritical pressures. Different from the subcritical phase transition process, Banuti [31] considered that supercritical pseudo-phase transition occurs in a finite temperature range $[T^-, T^+]$,
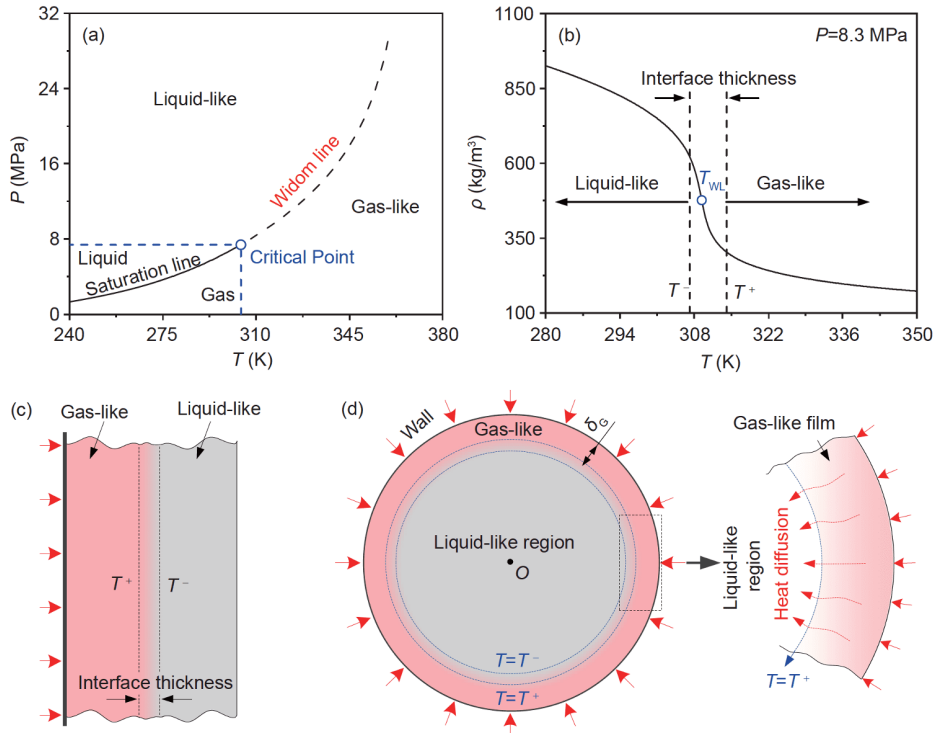
Figure 1 (Color online) Thermodynamics state and heat transfer behavior for sCO$_2$. (a) Phase transition at subcritical and supercritical pressures is characterized by *P-T* curve. (b) The transition between liquid-like phase and gas-like phase. (c) The process of liquid-like transiting to gas-like under heating condition. (d) The physical model to sCO$_2$ heat transfer in heated vertical tube.

and liquid-like transiting to gas-like starts at T^- and then terminates at T^+ under heating condition (see Figure 1(b) and (c)). The fluid is deemed as the perfect liquid-like phase at $T_f < T^-$, the fluid is deemed as the perfect gas-like phase at $T_f > T^+$. The narrow transition region where $T^- < T_f < T^+$ can be regarded as the thickness of interface between liquid-like and gas-like, where liquid-like and gas-like coexist. Zhu et al. [32] have quantitatively determined the T^- and T^+ for sCO$_2$ at the specified operating pressure.

According to Holman et al. [22] and Ackerman [23], the analogy to the subcritical inverted-annular film boiling model [33,34], the static heat transfer model of sCO$_2$ is established in the present study (see Figure 1(d)). The heat transfer region at the cross-section of circular tube is divided into two parts: gas-like region and liquid-like region. To understand the effect of gas-like film covering heated wall on heat transfer, the interface and core liquid-like regions ($T_f < T^+$) are regarded as a whole domain which is collectively referred to as liquid-like region in the present investigation. The process of heat transfer primarily includes two steps: heat from heated tube wall transferring to gas-like phase, and then from gas-like film transferring to liquid-like region. Obviously, the heat transfer ability of both gas-like film and core liquid-like will significantly affect temperature distribution along the heated wall.

Besides, Hsu and Westwater [35] proposed that the gas-liquid interface was generally under turbulence state when

inverted-annular film boiling occurred at subcritical pressure. It is easy to comprehend that turbulence intensity near the gas-liquid interface directly affects the heat transfer from the gas phase to the liquid phase. Similarly, during sCO$_2$ heat transfer, if the intensity of turbulence diffusion in the core liquid-like region is inferior, the heat transferring to the core region will be further suppressed after passing through the gas-like film. The heated wall will not be cooled effectively. Therefore, the effect of the above factors on heat transfer will be systematically considered in the present study.

3 Experimental measurement and numerical methodology

3.1 Experimental system and uncertainty analysis

In our previous investigation [36], the experimental loop system to sCO$_2$ heat transfer has been built to measure experimental data of sCO$_2$ flowing upward in a vertical tube and was reported in detail. That will not be represented here. Based on the above experimental system, the tube section is replaced to perform the experimental measurement of sCO$_2$ flowing downward in the vertical tube in the present study. The test tube with outer diameter of 14 mm and wall thickness of 2 mm is constructed of 1Cr18Ni9Ti (see Figure 2). The sCO$_2$ flows from the top of tube to the bottom. The length of heating section is 2000 mm. The inlet and outlet
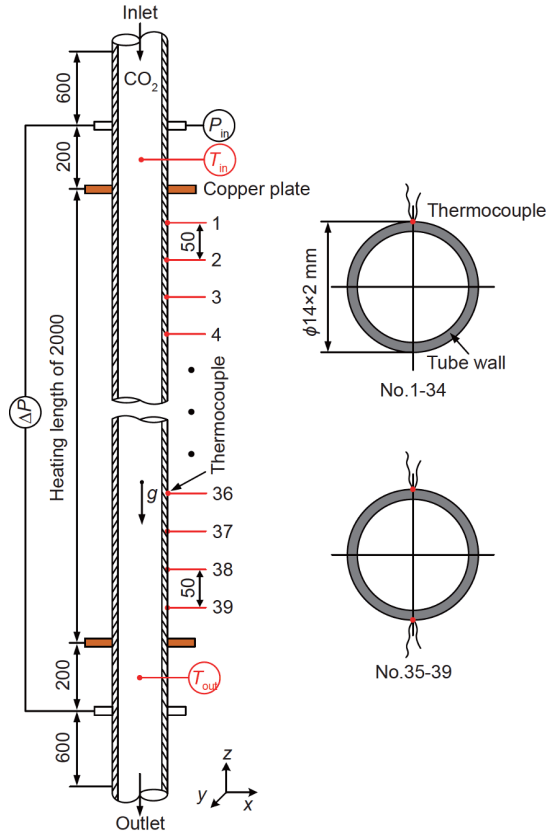
Figure 2   (Color online) Test section.

Table 1   Experimental parameters and uncertainties

Parameters (Unit)	Range	Uncertainty
Pressure P (MPa)	7.81–21.1	0.947%
Pressure difference (kPa)	5.1–49.4	2.01%
Inlet temperature T_{in} (°C)	20–42	0.5°C
Outlet temperature T_{out} (°C)	30–200	0.5°C
Outer wall temperature T_{wo} (°C)	40–420	0.5°C
Heat flux q_w (kW/m²)	50–369	5.12%
Mass flux G (kg/(m² s))	510–1250	1.99%
Heat transfer coefficient h (kW/(m² K))	0.909–12.23	5.37%

sections with a length of 800 mm are set before and after heating section to ensure full development at the inlet and stable flow at the outlet, respectively. Two copper plates are welded with the tube as electrodes for the electrical heating by DC power supply. In order to measure the local wall temperature, thirty-nine thermocouples are arranged with 50 mm interval at the outer wall along the tube. Although two thermocouples are welded on some specified cross-sections, the two indications are almost the same owing to the geometry symmetry. To ensure thermal efficiency of the test tube, the test section is enveloped by thermal insulation material whose thickness is 50 mm and thermal conductivity is as low as 0.036 W/m K. Similarly, the calculation methods of both data reduction and parameter uncertainties can be referred to the ref. [36]. The experimental parameters and uncertainties are briefly listed here (see Table 1).

3.2   Numerical methodology

3.2.1   Governing equations

The behavior of flow and heat transfer for sCO_2 in the vertical heated tube is simulated by ANSYS Fluent 15.0 software. The steady governing equations involving continuity, momentum and energy in the present investigation are expressed by Favre average form as below.

Continuity equation

$$\frac{\partial(\overline{\rho}\,\tilde{u}_i)}{\partial x_i} = 0, \tag{1}$$

Momentum equation

$$\frac{\partial\left(\overline{\rho}\,\tilde{u}_i\tilde{u}_j\right)}{\partial x_j} = -\frac{\partial\overline{p}}{\partial x_i} +$$

$$\frac{\partial}{\partial x_j}\left[\mu\left(\frac{\partial u_i}{\partial x_j} + \frac{\partial u_j}{\partial x_i} - \frac{2}{3}\delta_{ij}\frac{\partial u_k}{\partial x_k}\right) - \overline{\rho u_i'u_j'}\right] + \rho g_i, \tag{2}$$

Energy equation

$$\frac{\partial\left(\overline{\rho}\,\tilde{u}_i\tilde{h}\right)}{\partial x_i} = \frac{\partial}{\partial x_i}\left[\mu\left(\frac{1}{\mathrm{Pr}} + \frac{\mu_t/\mu}{\mathrm{Pr}_t}\right)\frac{\partial\tilde{h}}{\partial x_i}\right], \tag{3}$$

where "–" represents the time average scalar, "~" represents the Favre average scalar.

Besides, Wang et al. [37] evaluated the diversified turbulence models to obtain more accurate prediction results of sCO_2 heat transfer and found that the calculated values by SST k-ω low Reynolds turbulence model were closer to the experimental results. Therefore, the SST k-ω turbulence model is adopted in this paper and the transport equations are written as follows, respectively.

Turbulent kinetic energy equation

$$\frac{\partial(\overline{\rho}\,\tilde{u}_ik)}{\partial x_i} = \frac{\partial}{\partial x_j}\left[\left(\mu + \frac{\mu_t}{\sigma_k}\right)\frac{\partial k}{\partial x_j}\right] + G_k - Y_k. \tag{4}$$

Specific dissipation rate equation

$$\frac{\partial(\overline{\rho}\,\tilde{u}_i\omega)}{\partial x_i} = \frac{\partial}{\partial x_j}\left[\left(\mu + \frac{\mu_t}{\sigma_\omega}\right)\frac{\partial\omega}{\partial x_j}\right] + G_\omega - Y_\omega + D_\omega. \tag{5}$$

In eqs. (1)–(5), ρ, u, h, and μ represent the density, velocity, enthalpy and viscosity, respectively. The μ_t is the turbulent dynamic viscosity, and Pr_t is the turbulent Prandtl number. The function and constant terms in the above equations can be referred to the ref. [38].

3.2.2   Boundary condition and solution method

The simplified geometric model for simulating sCO_2 heat transfer adopted in this paper is exactly the same as in Ref. [24], it will not be shown here. The inlet type is the mass-

flow-inlet boundary, the outlet type is the pressure-outlet boundary. Both the wall of adiabatic sections corresponding to inlet and outlet are set as adiabatic boundary. The heat flux at the heated section is uniform and the fluid-wall is set as no slip shear condition. The SIMPLEC algorithm is adopted to pressure-velocity coupling scheme. The spatial discretization schemes adopt second order upwind to improve simulation accuracy. The values of residual convergence criterion for mass and momentum equations are set as 10^{-5}, and that for energy equation is 10^{-7}. The NIST real gas model in Fluent software is called to ensure the demand for physical properties of sCO_2 during the numerical simulation.

3.2.3 Grid generation and independence

The structured grids are generated by ANSYS ICEM 15.0 software (see Figure 3). The drastic change in physical property near the wall has a significant effect on heat transfer. Thereby, the more refined mesh is generated near

the fluid-wall region to predict accurately flow and heat transfer information. To satisfy the calculation requirements of the SST k-ω turbulence model, the non-dimensional wall distance y^+ is kept less than 1. The size between the inner wall and the first node is set as 0.0015 mm in the present simulation.

Besides, The grid independence analysis has been strictly implemented in our previous research (see ref. [24]), and the total number of grid nodes for numerical simulation is determined to be 2.08×10^6. The grid number is also employed in the present calculations.

3.2.4 Verification of numerical model

The experimental verification is very essential to ensure the reliability of numerical model and method. Figures 4 and 5 show the comparison between simulation and experiment data of sCO_2 flowing downward and upward, respectively. Meanwhile, mean relative error e_A and maximum relative
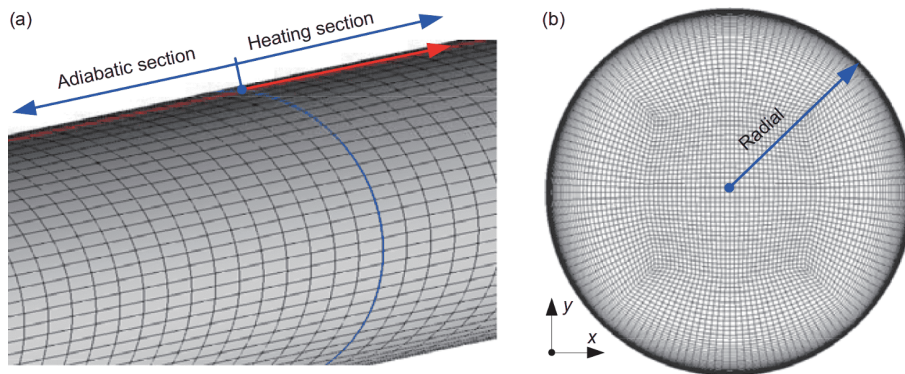

Figure 3 (Color online) Grid generation. (a) Grid generation along the axis; (b) grid generation in cross-section of circular tube.
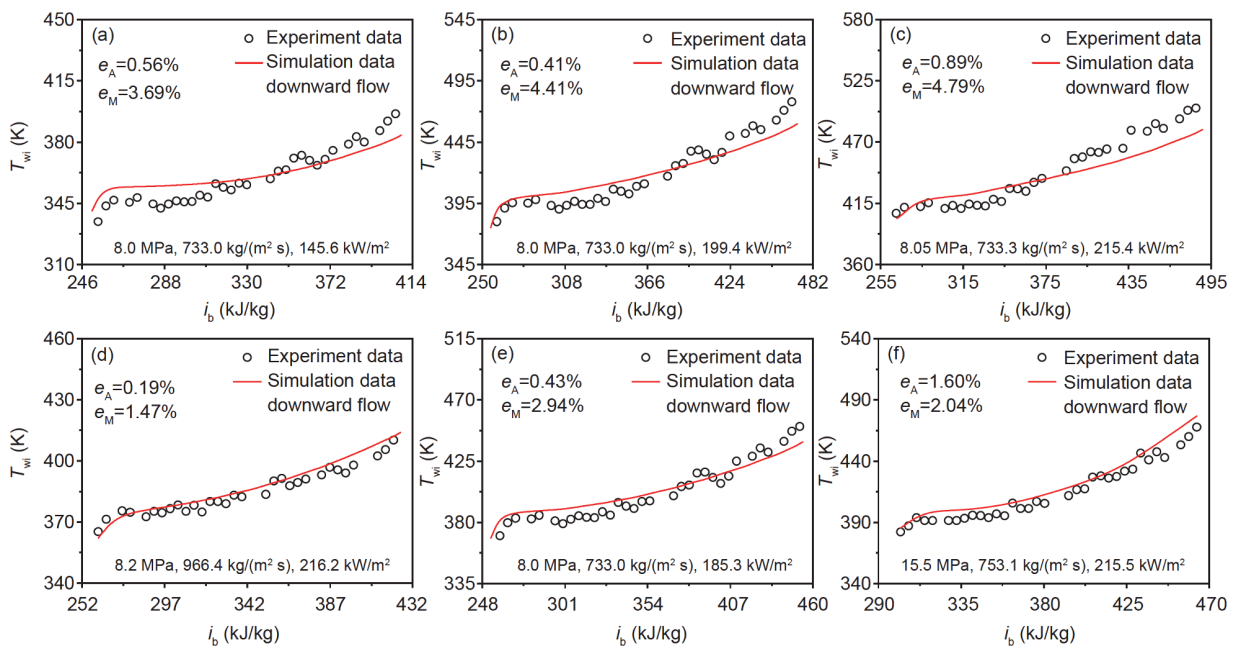

Figure 4 (Color online) Comparisons between simulation and experimental data in downward flow.
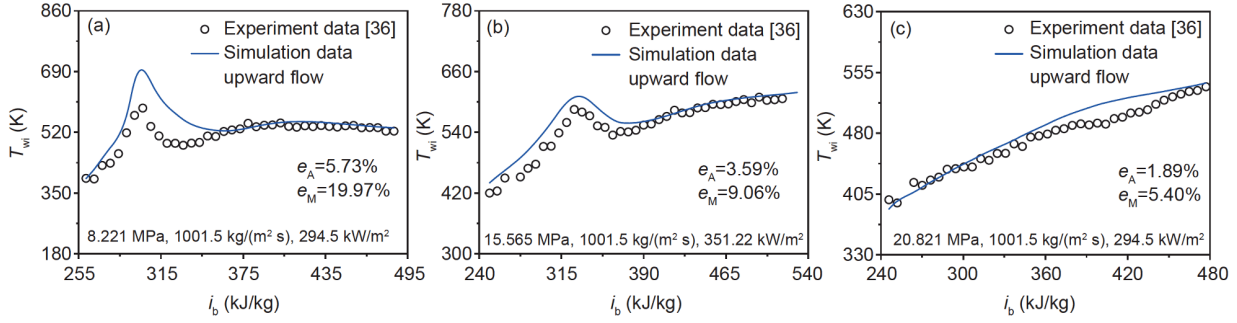
Figure 5 (Color online) Comparisons between simulation and experimental data in upward flow.

error e_M between the simulated data and the experimental data are also calculated. It can be found from Figures 4 and 5 that the calculated data display an acceptable consistency with experimental data that includes NHT mode and HTD mode. Therefore, the numerical model employed in the current investigation is reliable. It should be noted that the experimental data in Figure 4 where sCO$_2$ flows downward are collected through the test tube motioned in Section 3.1.

In Figures 4 and 5, e_A is calculated as below:

$$e_A = \frac{1}{n}\sum_{i=1}^{n} e_i \times 100\%, \tag{6}$$

where $e_i = |T_{pre} - T_{exp}|/T_{exp}$, which is only the error for a data point. And $e_M = \max(e_1, e_2, e_3, \ldots, e_i, \ldots, e_{n-2}, e_{n-1}, e_n)$.

4 Results and discussion

4.1 The effect of heat flux

In this section, the influence of heat flux on sCO$_2$ heat transfer is evaluated through two heat fluxes being q_w =210 kW/m^2 and q_w=260 kW/m^2. Figure 6(a)–(c) show the curves of inner wall temperature T_{wi} and heat transfer coefficient h under different heat fluxes, as well as the inner wall temperature difference ΔT_{wi} between upward flow and downward flow against bulk enthalpy i_b. ΔT_{wi} can intuitively reflect the difference between upward and downward flows and is defined as follow.

$$\Delta T_{wi} = T_{wi,u} - T_{wi,d}, \tag{7}$$

where $T_{wi,u}$ and $T_{wi,d}$ represent the inner wall temperature in upward flow and downward flow, respectively.

As shown in Figure 6(a) and (b), flow direction has a momentous effect on T_{wi} distribution. For vertical upward and downward flows, T_{wi} rises with the increase of heat flux. It becomes apparent that T_{wi} in downward flow is always lower than that in upward flow. A similar phenomenon was experimentally observed by Li et al. [27] and Jiang et al. [39]. On the contrary, h in both upward and downward flows decreases with the increase of heat flux. Simultaneously, h in downward flow is always higher than upward flow at the same heat flux and decreases uniformly along the circular
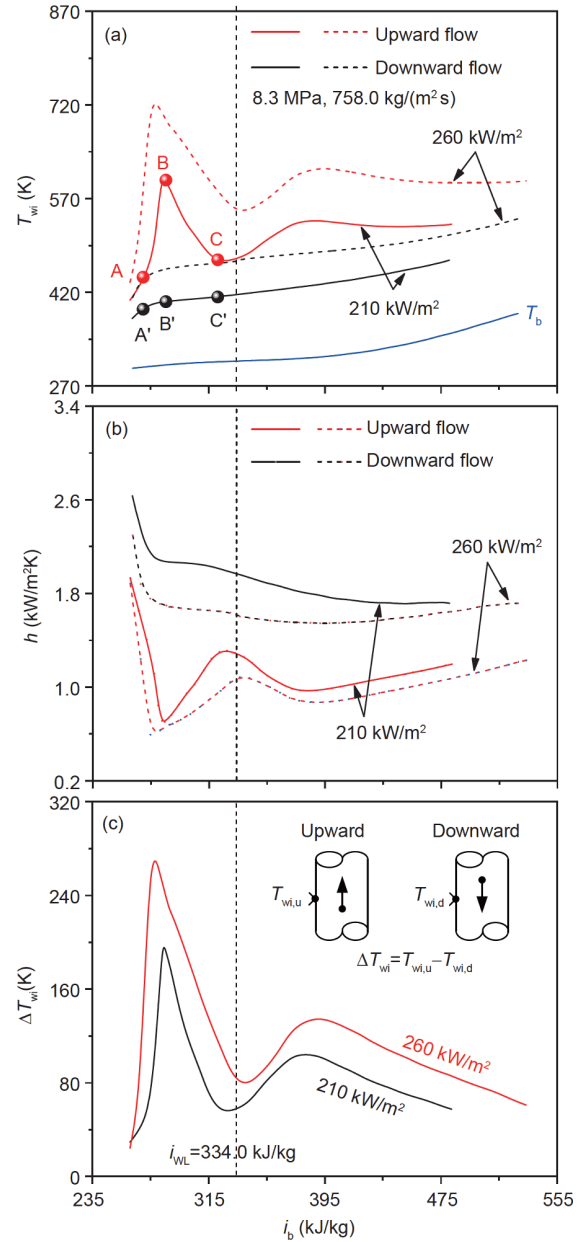

Figure 6 (Color online) Effect of heat flux on the distribution of inner wall temperatures and heat transfer coefficients in upward and downward flows.

tube. In vertical upward flow, the localized impairment that is characterized as a remarkable wall temperature peak occurs in the upstream region of pseudo-critical enthalpy i_{WL}. The temperature peak and its span will increase as q_w increases. However, T_{wi} shows a moderate change trend in downstream region of pseudo-critical enthalpy i_{WL}. T_{wi} in vertical downward flow rises monotonously without local wall temperature peak for all simulated cases, which is at NHT state. It illustrates that sCO$_2$ heat transfer in downward flow is superior, and the HTD can be effectively inhibited.

Besides, the level of ΔT_{wi} is higher as q_w increases (see Figure 6(c)), which implies that the larger q_w is, the greater the heat transfer difference between upward and downward flows is. The phenomenon also indirectly reflects that the larger q_w is, the more prominent effect of down-flow on restraining wall temperature is.
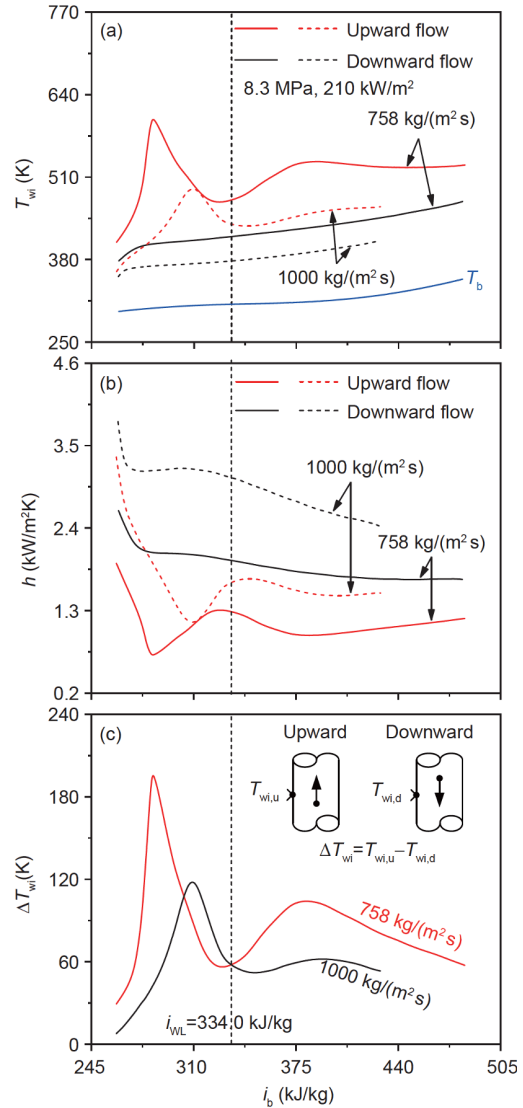
4.2   The effect of mass flux

The effect of mass flux is evaluated through two mass fluxes being G=758 kg/(m^2 s) and G=1000 kg/(m^2 s) at P=8.3 MPa and q_w=210 kW/m^2. As shown in Figure 7(a) and (b), T_{wi} decreases with the increase of mass flux in both vertical upward and downward flows, and h rises with the increase of mass flux. For upward flow, the degree of HTD can be reduced and even eliminated at higher mass flux. Moreover, the conclusion is consistent with Sect. 4.1 where T_{wi} in vertical upward flow is always higher than that in downward flow under the same operating parameter. The same numerical conclusion was also drawn by Guo et al. [40]. It further illustrates that the heat transfer performance of sCO$_2$ is always better than that in upward flow. In Figure 7(c), it can be found that higher mass flux results in less difference in the heat transfer performance and wall temperature distribution between upward and downward flows.

4.3   The effect of operation pressure

The effect of pressure on heat transfer is evaluated through two pressures being P=8.3 MPa and P=20.3 MPa at G=758 kg/(m^2 s) and q_w=210 kW/m^2. Figure 8(a) and (b) show T_{wi} decreases with the increase of operating pressure and heat transfer coefficient h increases. It can be seen that higher pressures can suppress the occurrence of HTD because HTD weakens and even disappears when pressure rises. Besides, ΔT_{wi} dwindles with operation pressure increasing, the effect of down-flow suppressing wall temperature rise is less remarkable at high supercritical pressure (see Figure 8(c)).

4.4   Analysis of heat transfer in vertical upward and downward flows

In this section, the cases (P=8.3 MPa, G=758.0 kg/(m^2 s), q_w

Figure 7   (Color online) Effect of mass flux on the distribution of inner wall temperatures and heat transfer coefficients in upward and downward flows.

=210 kW/m^2) for upward and downward flows in Figure 6(a) are chosen and characteristic points A and A′, B and B′, C and C′ are marked to reveal the reasons for sCO$_2$ heat transfer difference between upward and downward flows. Figure 9 displays the distribution of physical properties and turbulence flow at points A and A′. It can be observed that gas-like film with low-density is formed near the wall region in both upward and downward flows at the beginning of heat transfer and covers the heated wall. The difference of gas-like film between upward and downward flows is not obvious, but the gas-like film in upward flow is still slightly thicker and its properties characterized by specific heat at constant pressure c_p and thermal conductivity λ is slightly worse (see Figure 9 (a)–(c)). Meanwhile, turbulent kinetic energy k in upward flow is somewhat lower, especially in the core liquid-like region (see Figure 9(d)). Hence, compared with the down-
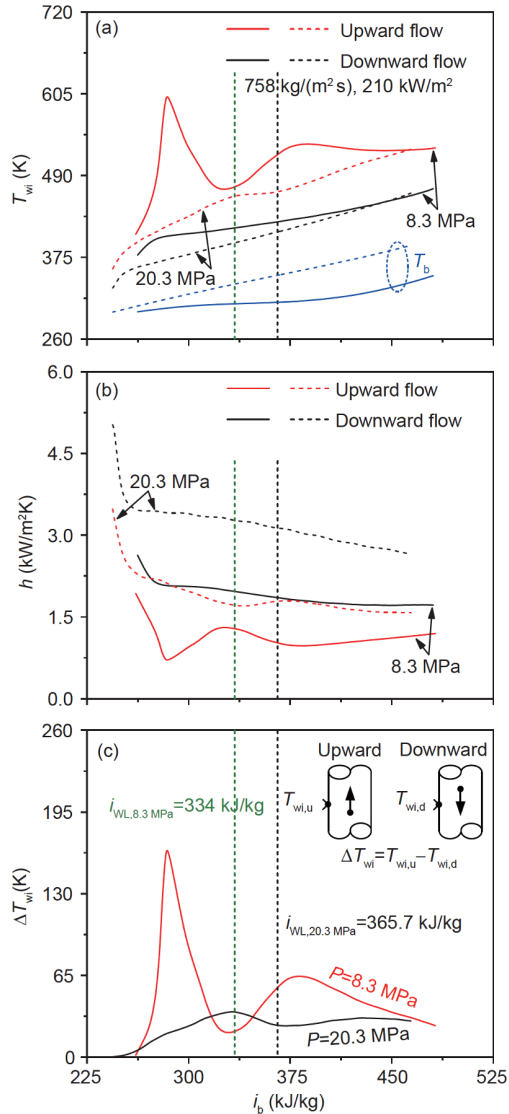
Figure 8 (Color online) Effect of pressure on the distribution of inner wall temperatures and heat transfer coefficients in upward and downward flows.

ward flow, the thermal resistances of both gas-like film and core liquid-like in upward flow will be greater. Since heat diffusion in the fluid domain is hindered layer by layer, which is responsible for the temperature at point A is higher than that at point A′.

Figure 10 displays the distribution of physical properties and turbulence flow at characteristic points B and B′. The key observation in Figure 10(a)–(c) is that the film thickness difference between upward and downward flows increases, and the gas-like film property in upward flow is worse. Inferior gas-like film results in its ability of heat absorption and thermal conductivity being weakened. Simultaneously, in upward flow, turbulent kinetic energy k near T^+ and in the core liquid-like region is dramatically lower, where it is revealed that the fluid almost approaches laminarization.

Owing to larger heat transfer resistances of both gas-like film and core liquid-like in upward flow, it is unfortunate that the heat from tube wall will be severely hindered from being diffused to the core liquid-like whose ability to transport heat is usually excellent. Consequently, the temperature at point B is higher than that at point B′, even the local HTD emerges in upward flow.

Figure 11 shows the distribution of physical properties and turbulence flow at points C and C′. It becomes apparent that the distribution characteristic of physical properties and turbulence flow at points C and C′ is similar to that at points B and B′. However, as a comparison with points B and B′, the level of turbulent kinetic energy k at both points C and C′ is improved. As we described in ref. [24], the increase of turbulent kinetic energy k may be one of the important reasons for wall temperature recovery after wall temperature rising sharply at the HTD stage.

As we all know, the wall temperature is affected by the promotion or inhibition of heat diffusion in the fluid region. However, the effect of thickness and property of gas-like film as well as turbulence intensity described in Figures 9–11 on heat transfer can only be qualitatively analyzed. In order to further explore quantitatively the effect of gas-like film and core liquid-like on the occurrence of HTD and the reasons why wall temperature T_{wi} in upward flow is always higher than that in downward flow, the thermal resistances of gas-like film and core liquid-like are proposed based on the pseudo-inverted-annular film boiling model established in Sect. 2. The thermal resistance of gas-like film R_G is defined as below:

$$R_G = \frac{\delta_G}{\lambda_{eff,G}}, \qquad (8)$$

where δ_G is the thickness of the gas-like film, namely the distance from the inner wall of tube to the location of T^+. $\lambda_{eff,G}$ is the effective thermal conductivity in the gas-like region.

The thermal resistance of core liquid-like R_L is expressed as below:

$$R_L = \frac{\delta_L}{\lambda_{eff,L}}, \qquad (9)$$

where δ_L is the distance between the location of T^+ and the center of liquid-like region, and $\lambda_{eff,L}$ is the effective thermal conductivity in the liquid-like region.

The effective thermal conductivity λ_{eff} can be expressed as below:

$$\lambda_{eff} = \lambda + \frac{c_p \mu_t}{Pr_t}. \qquad (10)$$

The λ_{eff} takes comprehensively molecular thermal conductivity and turbulence heat transfer into consideration. That being said that thermal resistance R reflects quantitatively the effect of multiple factors including fluid region thickness, fluid properties, and turbulence on heat diffusion.
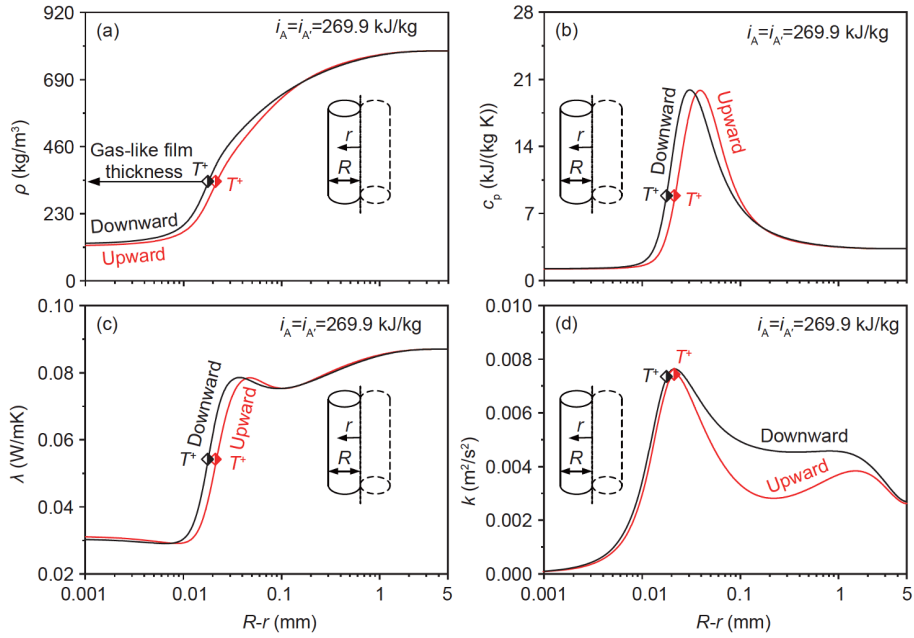
Figure 9 (Color online) The physical property and turbulent flow fields at characteristic points A and A′ in upward and downward flows. (a) Density; (b) specific heat; (c) thermal conductivity; (d) turbulent kinetic energy.
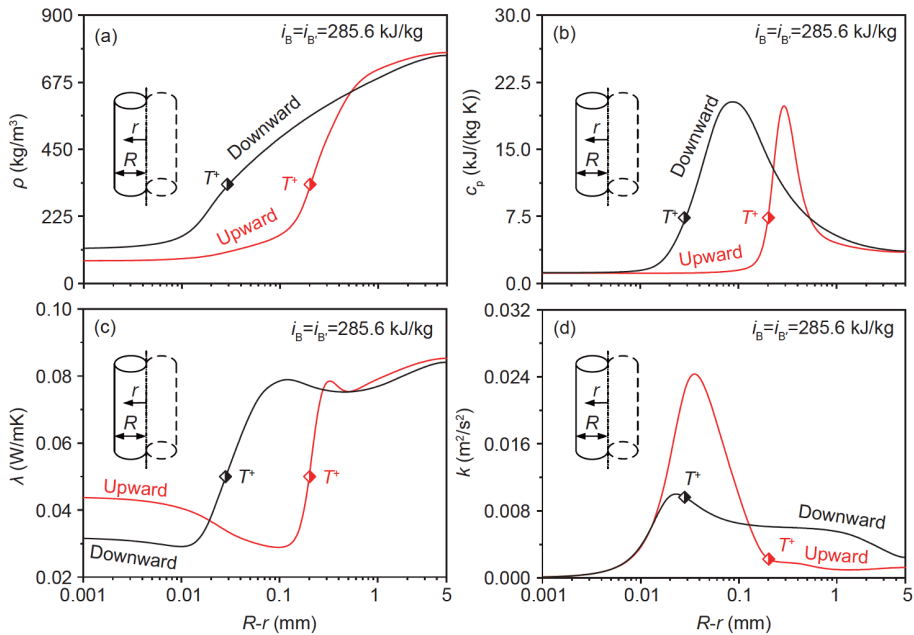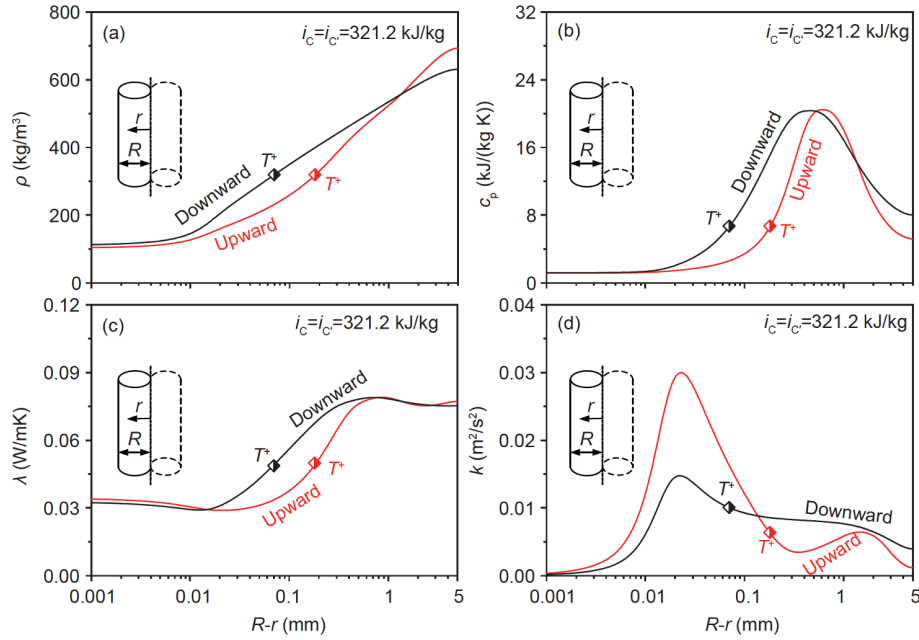

Figure 10 (Color online) The physical property and turbulent flow fields at characteristic points B and B′ in upward and downward flows. (a) Density; (b) specific heat; (c) thermal conductivity; (d) turbulent kinetic energy.

In Sect. 3.2, it is found that the numerical model can predict the experimental data in downward flow well when the turbulent Prandtl number in the energy eq. (3) was set to $Pr_t=0.74$. However, for upward flow, the simulation data is closer to the experimental data when the turbulent Prandtl number in the energy equation was set to $Pr_t=0.85$.

The local thickness variations of gas-like film $\delta_{G,u}$ in upward flow and $\delta_{G,d}$ in downward flow versus bulk enthalpy i_b are plotted in Figure 12(a). In general, $\delta_{G,u}$ is larger than $\delta_{G,d}$.

And $\delta_{G,u}$ has a pronounced peak value at point B, $\delta_{G,d}$ increases monotonously along bulk enthalpy. These curves emerge similar trends as T_{wi} changes shown in Figure 6(a). It is confirmed that there exists a close relationship between wall temperature distribution and gas-like film thickness.

For both upward and downward flows, a comparative analysis of thermal resistances including $R_{G,u}$, $R_{L,u}$, $R_{G,d}$ and $R_{L,d}$ along bulk enthalpy i_b is described in Figure 12(b). $R_{G,u}$ and $R_{G,d}$ represent thermal resistance of gas-like film in up-

Figure 11 (Color online) The physical property and turbulent flow fields at characteristic points C and C′ in upward and downward flows. (a) Density; (b) specific heat; (c) thermal conductivity; (d) turbulent kinetic energy.

ward and downward flows, respectively. $R_{L,u}$ and $R_{L,d}$ represent thermal resistance of core liquid-like in upward and downward flows, respectively. It can be observed that owing to the gas-like film being thin, heat transfer resistance is mainly concentrated in the core liquid-like region at the beginning of heating. Gradually, R_G becomes noticeably more and more dominant than R_L with the heating process, which is caused by gas-like film growing thicker. That means gas-like film plays a major role in sCO$_2$ heat transfer. Furthermore, $R_{G,u}$ and $R_{L,u}$ are always larger than $R_{G,d}$ and $R_{L,d}$, respectively. In other words, compared with the upward flow, whether passing through gas-like film covering the heated wall or core liquid-like region, heat from the heated wall always experiences less resistance in downward flow. And the changing trend of thermal resistance in downward flow is gentle. In contrast, thermal resistances $R_{G,u}$ and $R_{L,u}$ in upward flow change dramatically, especially when $i_b < i_{WL}$, where both $R_{G,u}$ and $R_{L,u}$ increase firstly and then decrease, and the maximum of both $R_{G,u}$ and $R_{L,u}$ correspond to the maximum T_{wi} at point B marked in Figure 6(a). In particular, it can be concluded that larger local $R_{G,u}$ in upward flow is the primary factor inducing the occurrence of HTD.

The relation between the total thermal resistance R_t and wall temperature T_{wi} in upward and downward flows is shown in Figure 12(c), where $R_t = R_G + R_L$. The comparison between $R_{t,u}$ and $R_{t,d}$ explains why the wall temperature distribution in downward flow is always well-behaved, and the heat transfer coefficient is higher than that in upward flow. It is an exciting phenomenon where the variation trend of $R_{t,u}$ is well identical with that of $T_{wi,u}$ in upward flow. $R_{t,u}$ presents a reliable prediction for the occurrence of HTD.

Therefore, the physical model established in Sect. 2, where the gas-like film region near the wall and core liquid-like region is divided, is verified to be reasonable. Due to $R_{t,d}$ increasing slightly, the wall temperature $T_{wi,d}$ at the entrance section rising steeply in downward flow. Then, $R_{t,d}$ generally decreases and is at a low level. It illustrates that because of sCO$_2$ bulk temperature increasing gradually, the decrease of cooling capacity is the predominant reason leading to $T_{wi,d}$ in downward flow increasing gently along with bulk enthalpy.

5 Conclusions

A numerical simulation of heat transfer for upward and downward sCO$_2$ flow is performed in the vertical heated tube. The thermal resistance mechanism is proposed to further explore the HTD mechanism and the reasons for heat transfer difference caused by flow direction. The main conclusions can be drawn as follows.

(1) Compared with the upward flow, superior heat transfer performance is exhibited when sCO$_2$ flows vertically downward and the occurrence of HTD may be avoided, where T_{wi} increases monotonically and heat transfer coefficient decreases monotonically along flow direction. However, The heat transfer difference between upward and downward flows is less when heat flux is low, mass flux and pressure are high.

(2) The fact that thermal resistance accurately predicts the occurrence of HTD proves the rationality and reliability of the pseudo-inverted-annular film boiling model and thermal resistance mechanism proposed in the present study. Relative
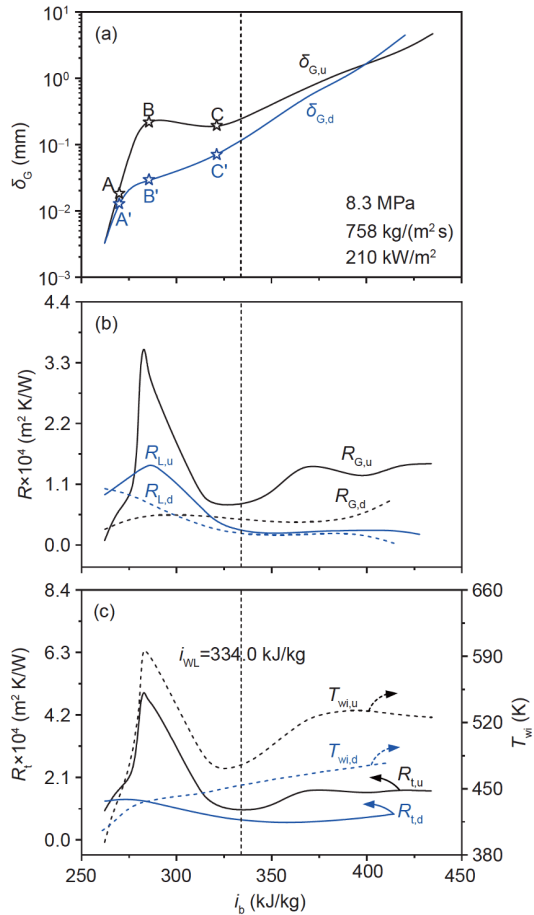
Figure 12 (Color online) Variations of thickness of gas-like film δ_G and thermal resistance R versus bulk enthalpy for upward and downward flows.

to thermal resistance in core liquid-like R_L, the effect of thermal resistance of gas-like film R_G on heat diffusion is dominant, especially, larger local R_G is the primary factor inducing HTD.

(3) Compared with the upward flow, due to smaller both R_G and R_L in downward flow, heat from the heated wall can effectively diffuse in the fluid region and be transported promptly, which reasonably explains why T_{wi} in downward flow is lower than that in upward flow.

(4) For downward flow, with the process of heating, due to total thermal resistance that is the sum of R_G and R_L being at a low level, the gentle increase of wall temperature is considered to be mainly caused by the decrease of fluid cooling capacity because of bulk temperature rising.

1 Dostal V, Driscoll M J, Hejzlar P. A supercritical carbon dioxide cycle for next generation nuclear reactors. MIT-ANP-TR-100, 2004

2 Xu J, Sun E, Li M, et al. Key issues and solution strategies for su-percritical carbon dioxide coal fired power plant. Energy, 2018, 157: 227–246

3 Lu S M. A global review of enhanced geothermal system (EGS). Renew Sustain Energy Rev, 2018, 81: 2902–2921

4 Zeyghami M, Khalili F. Performance improvement of dry cooled advanced concentrating solar power plants using daytime radiative cooling. Energy Convers Manage, 2015, 106: 10–20

5 Huang D, Wu Z, Sunden B, et al. A brief review on convection heat transfer of fluids at supercritical pressures in tubes and the recent progress. Appl Energy, 2016, 162: 494–505

6 Chen L F, Liu D, Zhang H L, et al. Theoretical investigations on heat transfer to H_2O/CO_2 mixtures in supercritical region. Sci China Tech Sci, 2020, 63: 1018–1024

7 Xu J, Liu C, Sun E, et al. Perspective of S-CO_2 power cycles. Energy, 2019, 186: 115831

8 Kim D E, Kim M H, Cha J E, et al. Numerical investigation on thermal-hydraulic performance of new printed circuit heat exchanger model. Nucl Eng Des, 2008, 238: 3269–3276

9 Wen Z X, Lv Y G, Li Q. Comparative study on flow and heat transfer characteristics of sinusoidal and zigzag channel printed circuit heat exchangers. Sci China Tech Sci, 2020, 63: 655–667

10 Pioro I L, Duffey R B. Experimental heat transfer in supercritical water flowing inside channels (survey). Nucl Eng Des, 2005, 235: 2407–2430

11 Bourke P J, Pulling D J, Gill L E, et al. Forced convective heat transfer to turbulent CO_2 in the supercritical region. Int J Heat Mass Transfer, 1970, 13: 1339–1348

12 Jiang P X, Zhang Y, Xu Y J, et al. Experimental and numerical in-vestigation of convectionheat transfer of CO_2 at supercritical pressures in a vertical tube at low Reynolds numbers. Int J Therm Sci, 2008, 47: 998–1011

13 Deng H, Zhu K, Xu G, et al. Heat transfer characteristics of RP-3 kerosene at supercritical pressure in a vertical circular tube. J Enh Heat Transf, 2012, 19: 409–421

14 Shiralkar B S, Griffith P. Deterioration in heat transfer to fluids at supercritical pressure and high heat fluxes. J Heat Transfer, 1969, 91: 27–36

15 Shiralkar B S, Griffith P. The effect of swirl, inlet conditions, flow direction, and tube diameter on the heat transfer to fluids at super-critical pressure. J Heat Transfer, 1970, 92: 465–471

16 Wang H, Bi Q, Yang Z, et al. Experimental and numerical in-vestigation of heat transfer from a narrow annulus to supercritical pressure water. Ann Nucl Energy, 2015, 80: 416–428

17 Fan Y H, Tang G H. Numerical investigation on heat transfer of supercritical carbon dioxide in a vertical tube under circumferentially non-uniform heating. Appl Therm Eng, 2018, 138: 354–364

18 Kim D E, Kim M H. Experimental investigation of heat transfer in vertical upward and downward supercritical CO_2 flow in a circular tube. Int J Heat Fluid Flow, 2011, 32: 176–191

19 Shen Z, Yang D, Wang S, et al. Experimental and numerical analysis of heat transfer to water at supercritical pressures. Int J Heat Mass Transfer, 2017, 108: 1676–1688

20 Zhang S J, Xu X X, Liu C, et al. Experimental investigation on the heat transfer characteristics of supercritical CO_2 at various mass flow rates in heated vertical-flow tube. Appl Therm Eng, 2019, 157: 113687

21 Xie J, Liu D, Yan H, et al. A review of heat transfer deterioration of supercritical carbon dioxide flowing in vertical tubes: Heat transfer behaviors, identification methods, critical heat fluxes, and heat transfer correlations. Int J Heat Mass Transfer, 2020, 149: 119233

22 Holman J P, Rea S N, Howard C E. Forced convection heat transfer to Freon 12 near the critical state in a vertical annulus. Int J Heat Mass Transfer, 1965, 8: 1095–1102

23 Ackerman J W. Pseudoboiling heat transfer to supercritical pressure water in smooth and ribbed tubes. J Heat Transfer, 1970, 92: 490–497

24 Yan C, Xu J, Zhu B, et al. Numerical analysis on heat transfer char-acteristics of supercritical CO_2 in heated vertical up-flow tube. Ma-

terials, 2020, 13: 723

25 Liao S M, Zhao T S. An experimental investigation of convection heat transfer to supercritical carbon dioxide in miniature tubes. Int J Heat Mass Transfer, 2002, 45: 5025–5034

26 Jiang P X, Zhang Y, Shi R F. Experimental and numerical investigation of convection heat transfer of CO_2 at supercritical pressures in a vertical mini-tube. Int J Heat Mass Transfer, 2008, 51: 3052–3056

27 Li Z H, Jiang P X, Zhao C R, et al. Experimental investigation of convection heat transfer of CO_2 at supercritical pressures in a vertical circular tube. Exp Therm Fluid Sci, 2010, 34: 1162–1171

28 Gorelli F, Santoro M, Scopigno T, et al. Liquidlike behavior of supercritical fluids. Phys Rev Lett, 2006, 97: 245702

29 Simeoni G G, Bryk T, Gorelli F A, et al. The Widom line as the crossover between liquid-like and gas-like behaviour in supercritical fluids. Nat Phys, 2010, 6: 503–507

30 McMillan P F, Stanley H E. Going supercritical. Nat Phys, 2010, 6: 479–480

31 Banuti D T. Crossing the widom-line-supercritical pseudo-boiling. J Supercrit Fluids, 2015, 98: 12–16

32 Zhu B, Xu J, Yan C, et al. The general supercritical heat transfer correlation for vertical up-flow tubes: *K* number correlation. Int J Heat Mass Transfer, 2020, 148: 119080

33 Elias E, Chambré P. Inverted-annular film boiling heat transfer from vertical surfaces. Nucl Eng Des, 1981, 64: 249–257

34 Hammouda N, Groeneveld D C, Cheng S C. Two-fluid modelling of inverted annular film boiling. Int J Heat Mass Transfer, 1997, 40: 2655–2670

35 Hsu Y Y, Westwater J W. Approximate theory for film boiling on vertical surfaces. Chem Eng Progress, 1960, 56: 15–24

36 Zhu B, Xu J, Wu X, et al. Supercritical "boiling" number, a new parameter to distinguish two regimes of carbon dioxide heat transfer in tubes. Int J Therm Sci, 2019, 136: 254–266

37 Wang K, Xu X, Wu Y, et al. Numerical investigation on heat transfer of supercritical CO_2 in heated helically coiled tubes. J Supercrit Fluids, 2015, 99: 112–120

38 Menter F R. Two-equation eddy-viscosity turbulence models for engineering applications. AIAA J, 1994, 32: 1598–1605

39 Jiang P X, Zhang Y, Zhao C R, et al. Convection heat transfer of CO_2 at supercritical pressures in a vertical mini tube at relatively low Reynolds numbers. Exp Therm Fluid Sci, 2008, 32: 1628–1637

40 Guo J, Xiang M, Zhang H, et al. Thermal-hydraulic characteristics of supercritical pressure CO_2 in vertical tubes under cooling and heating conditions. Energy, 2019, 170: 1067–1081